Manuscript prepared for Nat. Hazards Earth Syst. Sci. Discuss.
with version 4.1 of the LaTeX class copernicus_discussions.cls.
Date: 22 October 2014

Evaluating intense precipitation in high-resolution numerical model over a tropical island: impact of model horizontal resolution

N. Yu[1], C. Barthe[1], and M. Plu[1,*]

[1]Laboratoire de l'Atmosphère et des Cyclones (LACy) - UMR8105, CNRS, Université de la Réunion and Météo-France, Saint Denis, La Réunion, France
[*]Now at the Centre National de Recherches Météorologiques CNRM/GAME, CNRS and Météo-France, Toulouse, France

Correspondence to: Nan YU
(nan.yu@meteo.fr)

Abstract

A test of sensitivity to the model grid spacing for extreme rainfall simulation is carried out for the tropical island of La Réunion, which holds several world records of precipitation. An extreme rain event that occurred during the moist season in 2011 is selected to study the numerical model behavior at four horizontal resolutions: 4 km, 2 km, 1 km and 500 m. The assessment based on raingauge network shows that the performance of daily rain simulation increases as reducing the model grid spacing from 4 km to 1 km. The spatial variability of 24 h rainfall is well captured by the simulation at 1 km and 500 m resolution. However, refining the resolution from 1 km to 500 m has little impact on the model performance. Diagnosis analysis and numerical experiment reveal that only the 1 km and 500 m grid spacings are able to simulate a cold pool located near the coastal area of the island. This cold pool triggers the thermal lifting and creates convergence between the prevailing moist flow and offshore land breeze. The observed precipitation, air temperature and wind confirm the cold pool feature in simulation. However, this cold pool is missed in the 4 km and 2 km simulations. The numerical experiment highlights the important role of evaporation process at 1 km scale to create cold pool in simulating such intense precipitation.

1 Introduction

Recent progress in hydro-meteorological research and forecasting has been achieved thanks to significant improvements in numerical modeling of meso- and convective-scale dynamics and processes. Dramatic increase in processing power of super-computers has enabled numerical simulations of the atmosphere at very fine grid spacing. Many meteorological forecasting centers now operate models at kilometer scale resolution, such as the 2.5 km grid spacing model AROME used by Météo-France (Seity et al., 2011). Past experiences in hydrological modeling have emphasized the need for precise precipitation data in hydrological models (Kobold and Suselj, 2005). Reliable spatial and temporal distribution of convective rainfall is particularly essential for flooding prediction in small mountainous catchment (Bell and Moore,

2000; Tetzlaff and Uhlenbrook, 2005; Younis et al., 2008), where the flash floods may often cause serious water damages to property and even also loss of human life.

Previous investigations based on non-hydrostatic simulations have shown the advantages of high resolution models in capturing the detailed evolution and structure of convective systems. Contrary to coarse resolution simulations with convective parameterization, the high resolution models allow convective overturning to be resolved in an explicit manner. Weisman et al. (1997) suggested that the grid spacing of the numerical model should be reduced to 4 km to resolve explicitly Mesoscale Convective Systems (MCS). Bernardet et al. (2000) emphasized further the need of a 2 km grid spacing with a good representation of topographical features to simulate local MCS and supercell thunderstorms. Bélair and Mailhot (2001) studied the MCS dynamics using different model resolutions: 50, 18, 6 and 2 km. Only the 2 km configuration simulated well the leading band structure of convective systems. Colle et al. (2005) simulated a mountain blocking case and found that a horizontal grid spacing of 1.33 km is required to represent correctly precipitation over the central mountains. Luna et al. (2011) simulated an extreme rain event over a subtropical island and highlighted the significant improvement of the simulation with 1 km resolution comparing to 5 km. Smith et al. (2012) showed that decreasing grid spacing down to 1.5 km is beneficial for orographic precipitation forecast over the UK. Kendon et al. (2012) studied the realism of rainfall in 1.5 and 12 km regional climate model. They found that 1.5 km model gives a much better representation of the duration and spatial extent of heavy rainfall event as well. Furthermore, Petch et al. (2002); Petch (2006); Bryan (2003) and Craig and Dornbrack (2008) argued that even smaller grid spacing (less than 1 km) is still necessary to reproduce properly some convective processes, such as the heterogeneous heating over the land, the boundary layer eddies, the entrainment and the detrainment in clouds etc. Recently, Zhang and Zhang (2012) simulated a MCS along a stationary front with an extension up to 1000 km. They emphasized that even for such large scale system, the grid spacing below 1 km is necessary to represent well the cold dome left by previously dissipated MCS.

Despite the more realistic representation of physical processes in the finer models, there remains considerable doubt regarding their improvement on precipitation simulations and forecasts (Done et al., 2004). Mass et al. (2002) evaluated the forecast accuracy of a mesoscale

model (MM5) at 36, 12 and 4 km horizontal resolution over several years. They found an overall higher performance for the forecast with 12 km grid spacing, except that the 4 km model enhances the accuracy for heavy precipitation on the windward slopes of mountains. During the NOAA Hazardous Weather Testbed Spring Experiment, Kain et al. (2008) and Schwartz et al. (2009) indicated that decreasing horizontal grid spacing from 4 to 2 km provides little improvement on rainfall forecast in the United States. Chan et al. (2012) compared simulations of moderate and high daily precipitation events over the southern UK using three different resolutions (50, 12 and 1.5 km). They did not found clear evidence that the 1.5 km simulation is superior to the 12 km one at the daily precipitation level.

The benefits of high-resolution model seem to be highly case and geographically dependent. Mass et al. (2002) concluded that the high resolution simulation appears to be particularly useful for strongly forced convections (e.g. topography, fronts, heterogeneous heating between land and ocean, etc.). In the light of their conclusion, La Réunion Island is a good natural laboratory to study the sensitivity of intense rainfall simulation to the model resolution. This tropical mountainous island often suffers from torrential rain events. Some of its raingauges hold world records for the most rain falling over periods of 12 to 96 h (Quetelard et al., 2009). The current study is the first one that investigate precipitation modeling over this territory.

A research model with different horizontal grid spacings, from 4 km to 500 m, was used to simulate an extreme event at La Réunion during the moist season. The heavy rainfall event characterized by strong convection with topographic blocking process will be described in Sect. 2. In Sect. 3, we will focus on the assessment of rainfall simulations through a raingauge network. The spatial rain field over different cumulative periods (from 6 h to 48 h) and the extreme rainfall at particular locations will be separately considered in the evaluation. Following these results, the impact of model resolution on rainfall simulation and the underlying mechanism will be discussed in Sect. 4. The final objective is to investigate the model behavior at different resolutions and to understand the impact of resolution on physical processes in simulations.

2 Rain event description and model settings

2.1 Meteorology of the January 2011 rain event

La Réunion Island is located in the Indian Ocean, off the eastern coast of Madagascar (Fig. 1). This French volcanic island is about $63\,\mathrm{km}$ long and $43\,\mathrm{km}$ wide, with a surface area of $2512\,\mathrm{km}^2$. Two mountain summits, Piton des Neiges ($3072\,\mathrm{m}$) and Piton de la Fournaise volcano ($2611\,\mathrm{m}$), are located at the center and along the southeastern side of the island, respectively (Fig. 2b). The topography of the island is marked by many steep slopes and rugged valleys. Three calderas are enclosed by mountains and tall cliffs in the interior. The territory is submitted to various precipitation regimes including heavy rainfall associated with strong deep convection (Réchou et al., 2013). The heavy rainfall event that occurred between the 27th and the 30th of January 2011 will be studied hereafter using numerical simulations. During the four days, the maximum cumulative rainfall measured by a raingauge reached up to $1075\,\mathrm{mm}$, and 33 raingauge stations recorded more than $400\,\mathrm{mm}$ of precipitation. The traffic and electricity services were seriously disrupted due to the floods and rock slides, which caused one victim dead.

The large-scale synoptic setting for this event is showed in Fig. 1. The Aladin-Réunion analysis Montroty et al. (2008) indicates a weak depression developing near Madagascar, and a prevailing north-westerly moist flux over La Réunion on 28 January 2011 (Fig. 1b). This depression moved firstly toward the south-east, approaching to La Réunion on 29 (Fig. 1c), and then it was enforced and changed direction to the south-south-west (Fig. 1d). Warm and moist air coming from tropical regions lead to favorable conditions for developing convection. Figure 2a shows the four-days (from 27 January 00:00 UTC to 31 January 00:00 UTC) cumulative precipitation measured by 73 raingauges and estimated by S-band weather radar. Most of the northern area of the island was swept by intense precipitation ($> 900\,\mathrm{mm}\,(4\,\mathrm{days})^{-1}$), while relatively small rainfalls were observed in the south. For the radar rainfall estimation, we note a large overestimation in the northern coastal area, and also an underestimation on the lee side of mountains. These errors may be explained by beam blockages, ground clusters (Pellarin et al., 2002), incorrect attenuation corrections (Delrieu et al., 2000) and no-adapted reflectivity (Z) – rain intensity

(R) relationship for such tropical intense rain event (Yu et al., 2012). To avoid these errors in the assessment, only the raingauges observations will be used to evaluate explicitly the numerical simulations in the Sect. 3.

2.2 Model configuration

The numerical model Meso-NH (Lafore et al., 1998) jointly developed by Centre National de la Recherche Météorologique (Centre National de la Recherche Scientifique and Météo-France) and Laboratoire d'Aérologie (Centre National de la Recherche Scientifique and Université de Toulouse) is based on non-hydrostatic equations and it can deal with atmospheric systems at different sizes, ranging from synoptic to large eddy scales. For the simulations of rainfall, 70 model levels with variable spacing were defined in the vertical direction. The first vertical grid point was $20\,\mathrm{m}$ above the ground and the vertical grid length was defined by a logarithmic function. Four horizontal grid definitions (4km, 2km, 1km and 500m) were investigated in this study. First, several configurations of domain size and location were tested. Based on the results and our modeling experience, we selected four configurations to present the impacts of model resolution. The first two simulations at 4 and $2\,\mathrm{km}$ grid spacing were carried out within a large domain (D1: $360\,\mathrm{km} \times 360\,\mathrm{km}$, see red rectangle in Fig. 1). With the D1 as father domain, a nested domain (D2: $80\,\mathrm{km} \times 72\,\mathrm{km}$) with finer resolutions (1 km or 500 m) was then implemented.

The precipitation simulations under investigation began at 00:00 UTC, on 27 January 2011 and ran for 96 h (4 days). The Aladin-Réunion operational analyses at 8 km resolution were used to initialize the simulations and update the boundary conditions every six hours. The two-way nesting technique (Stein et al., 2000) was applied for the nested runs (1 km and 500 m). A one-moment, six-class hydrometeors microphysics scheme is implemented in the model (Pinty and Jabouille, 1998). The unified scheme both for mesoscale and large-eddy simulations developed by Cuxart et al. (2000) is applied to resolve turbulence in one- or three-dimensions. The shallow convection scheme (EDKF) combining eddy diffusivity transfers and mass flux transfers described by Pergaud et al. (2009) is activated in the model to resolve the subgrid-scale convective processes. A preliminary assessment of deep convection and of shallow con-

vection parameterizations on rainfalls was performed. The results showed that the parameterization of deep convection degrades our simulations, and the shallow convection scheme has a smaller impact on rain simulations comparing to the effect of model resolution. Hence, the deep-convection scheme was not used in any of these simulations while the shallow convection scheme EDKF was active in all the simulations. The different model configurations are listed in Table 1. Detailed studies about the turbulence and kinetic energy spectra as a function of resolution were carried out by Honnert et al. (2011) and Ricard et al. (2013).

3 Evaluation of model precipitation by the raingauge observations

3.1 Evaluation of the precipitation fields

Firstly, the spatial distribution of cumulative rainfall is analyzed and compared to raingauge observations. The 4 day rainfall produced by each simulation is illustrated in Fig. 3 accompanied with raingauges measurements. As a general comment, we obtain similar rainfall patterns in the 4 km and 2 km runs. The maximum simulated precipitation exceeding 900 mm is located in the east volcanic area, where neither the raingauge, nor the weather radar observed such strong rainfall at this location. Large underestimations are found in the northern coastal areas of the island. In the 2 km simulation, an intense rain zone ($R > 800\,\mathrm{mm}$) appears in the northern mountainous area, but both its intensity and coverage are smaller than the raingauges measurements. When decreasing the grid spacing from 2 km to 1 km and 500 m, the spatial distribution of precipitation is significantly affected: the rain peak near the volcano is totally removed and the precipitation in the north is significantly enforced. These spatial distributions of rainfall simulations are more consistent with the raingauges and radar observations.

The simulated precipitation fields during 24 h are then interpolated to the raingauges locations by a bilinear interpolation algorithm. Figure 4 shows the plot of simulated daily precipitation vs. observations for all raingauges stations. The brown and blue scatters indicate the intense rainfall (more than half of raingauges recorded at least 100 mm rain per day) on the third and fourth days of the event. A significant negative bias is obtained for the coarse resolution simulations (4 km

and 2 km) on the fourth day. At some stations, the observed daily rainfall is six times higher than the simulated daily rainfall. This negative bias was apparently reduced by the 1 km and 500 m runs. In order to evaluate these scatters in an objective manner, we introduce the spatial correlation coefficient and bias defined as:

$$R^2 = \frac{\sum_{i=1}^{n}(E_i - \overline{E})(O_i - \overline{O})}{\sqrt{\sum_{i=1}^{n}(E_i - \overline{E})^2 (O_i - \overline{O})^2}} \tag{1}$$

$$\text{Bias} = \frac{\overline{E}}{\overline{O}} - 1 \tag{2}$$

where E_i and O_i represent the estimated and observed rainfall at raingauge station i, respectively. n is the total number of available raingauges and overbar represents the spatially average of precipitation field. Figures 5a and 6a compare the two scores as a function of different grid spacings. The 500 m and 1 km runs simulate the intense precipitation on the last day with smaller bias (10 %) and higher correlation coefficients (0.8), while the simulations with coarser resolutions produce an important underestimation. This is consistent with the scatters shown in Fig. 4. However, we note that all runs underestimate the rainfall by about 20 % on the third day, with a slight improvement in the 500 m simulation. Regarding the cumulative rainfall during 12 h, the improvement by refining grid spacing becomes less apparent (Figs. 5b and 6b). Sometimes, the coarse resolution simulations yield a better performance than finer ones, which suggests that the temporal resolution of the rainfall has also a critical impact in rainfall assessment. A common shortcoming in all simulations is concerned with the size of the domain. The depression system is eventually out of simulated window and its information is only provided by the analysis fields every 6 hours. A larger domain covering this depression would be expected to improve the temporal accuracy of simulation at a cost of huge computer resource.

In order to focus on the model performance during the extreme rainy days and to simplify the assessments, we merged the data on the last two days together and calculated the simulated and observed rainfalls over 48, 24, 12 and 6 h at each raingauge station. The spatial correlation coefficient defined in Eq. (1) and the variation coefficient of the root-mean-square error (CVRMSE)

defined as

$$\mathrm{CVRMSE} = \frac{\sqrt{\frac{\sum_{i=1}^{n}(E_i - O_i)^2}{n}}}{\overline{O}} \tag{3}$$

are used as scores in the following. In Eq. (3), the value of n depends on the cumulative period. For 48 h rainfall, n is equal to the number of raingauge stations; n will multiply by 2 if the cumulative period is reduced to 24 h. The CVRMSE (without dimension) score reflecting the mean estimated error normalized by the average rainfall, allows a comparison of simulation errors among 48, 24, 12 and 6 h precipitation. The objective of the assessment is to demonstrate the model performance as a function of grid spacing and cumulative period for intense rainfall in ignoring the daily distinctions of this event.

Taking the inherent spatial and temporal variability of the rainfall into account, we construct two reference scores as criteria for the evaluation. Firstly, we consider the spatially average rainfall as rain estimations at all raingauge stations, and the variation coefficient of the rootmean-square deviation (CVRMSD) can be calculated by

$$\mathrm{CVRMSD} = \frac{\sqrt{\frac{\sum_{i=1}^{n}(\overline{O} - O_i)^2}{n}}}{\overline{O}}. \tag{4}$$

Regarding the reference score for evaluating the correlation coefficient, we create a persistence model to estimate the rainfall over Δt at t based on the previous observation at $t - \Delta t$

$$O_t = O_{t-\Delta t} \tag{5}$$

where by definition the Δt can be 48, 24, 12 and 6 h. The correlation coefficient reference is then calculated through Eq. (1) by setting E_i equal to O_t. Figure 7 shows the evaluation results. As expected, the numerical model performance decreases rapidly as reducing the cumulative period. Simulated errors in the 48 h and 6 h precipitation with the same grid spacing ($500\,\mathrm{m}$) increases from 35 % to 135 %. The reference scores reflecting the inherent variability of rainfall

exhibit the similar behaviors as numerical simulations. High CVRMSD value and low correlation coefficient for the 6 h precipitation suggest the large spatial and temporal variability in such observed rainfall. Comparing the model scores to the statistical reference scores, none of the numerical run can simulate the rainfall significantly better than the statistical scores for the 12 and 6 h rainfall. In another word, the refining of model grid spacing has little impact on performance for such short period precipitation. However, regarding the 48 h and 24 h rainfall, the two scores exhibit a robust sensitivity to the model resolution. The performance of numerical model is improved if small grid spacings are used in the simulations. The simulated error of daily precipitation decreases from 95 % to 55 % and the correlation coefficient increases from 0.35 to 0.8 by reducing the grid spacing from 4 km to 1 km. For the 1 km and 500 m runs, we do not find significant difference between them in the current assessment. The simulation performance is saturated at 1 km resolution. This saturation may be explained by the insufficient density of raingauge network and/or by the model ability. A radar rainfall estimation is needed in the future to assess these fine resolution models.

3.2 Precipitation at individual raingauge stations

The previous evaluation was mainly based on the information of the space-averaged rain intensity. Observations at all raingauge stations were used together to yield a global performance score for the entire rain field. However, this method ignores the extreme rainfall values at particular raingauge locations, which are important for flood simulations. A plot of quantile vs. quantile is used here to evaluate the simulation for the intense precipitation on the last two days of the event. We calculate the minimum value, the maximum value and the quantiles (from 10 % to 90 %) based on the observed and simulated cumulative distribution functions (CDF) of rainfall at all raingauge locations, respectively. These quantiles values are plotted on a XY diagram to compare the modeled and observed rain CDFs in Fig. 8. Consistently with the previous results illustrated in Fig. 5a, all runs underestimate the daily rainfall on the third day. 20 % of the stations records are greater than 200 $\mathrm{mm\,day^{-1}}$, whereas the 80 % quantile of simulations is around 110 $\mathrm{mm\,day^{-1}}$. The daily rainfall greater than 200 $\mathrm{mm\,day^{-1}}$ is slightly improved at some locations by reducing the model resolution to 500 m. For the intense rainfall on the last

day, the finer resolution models (500 m and 1-km) exhibit a significant improvement compared to the coarser resolution simulations. A nearly perfect quantile relationship between simulations and observations is obtained in these simulations. For the 4 km and 2 km simulations, even if the maximum simulated rainfalls agree well with the observations, they underestimate systematically the extreme rainfall between 50 $\mathrm{mm\,day^{-1}}$ and 250 $\mathrm{mm\,day^{-1}}$ at many raingauge locations. The quantile diagram confirms that the extreme rainfall simulations at particular positions also benefit from refining the grid spacing to 1 km.

The simulated and measured precipitation during the 4 days for each raingauge is calculated. The ratio of simulation to observation is showed, in Figure 9, as a function of the altitude and affiliated zone of raingauge (see the definition of these zones in Fig. 2b). Large negative biases in 4 km and 2 km simulations are revealed at raingauges located in the north and north-east, where the most intensive rainfall were recorded during this event. Additionally, these biases seem to be related to the altitude of the location: the rainfall tends to be underestimated at lower stations while it tends to be overestimated at higher locations. Reducing the grid spacing to 1 km again removes significantly the negative bias in simulations, especially over the northeast of the island.

4 Interpretation of the improvement for simulations at high resolution

The evaluations revealed similar behaviors between the 1 km and 500 m runs. Regarding the intense rainfall on the last day, 1 km seems to be a critical resolution to simulate the correct position and intensity of heavy precipitation. In this section, we will focus on the physical process explaining the sensitivity of rain simulation to model horizontal resolution.

The simulated horizontal wind field along with potential temperature at 950 hPa is shown in Fig. 10 for the 2 km-, 1 km- and 500 m-runs. A relative cold area is located at the north-east of the island in the 1 km- and 500 m-runs. The contrast in temperature between the cold area and the ocean yields an offshore breeze blowing from the coastal region to the ocean. The convergence between the cold land breeze and prevailing warm wind coming from the ocean triggers firstly adiabatic rising motions (Fig. 11) in the lower layers of the atmosphere. The

moist air flow with weak convective inhibition could rapidly reach to saturation and release latent heat as a source of energy for the development of deep convection at high altitude. As a result, a strong precipitation system is formed over this cold pool near the coastal area. The rainfall observed by the radar confirms the presence of the convective systems to the north-east of the island (Fig. 10d). However, the simulations at coarser resolutions (4 km and 2 km) are not able to simulate the cold pool and the northerly airflow penetrates directly the interior of the island. The main mechanism to trigger the precipitation in these coarse runs is only related to the orographic lifting. Consequently, the coarse resolution simulations produce an important underestimation of rainfall over the coastal area, with less negative bias for the precipitation over the mountainous region (Fig. 9).

Figure 12 shows the observed series of average temperature and surface wind at two meteorological stations located in the north of Réunion Island (see the positions in Fig. 10d) on the last day. The 2 m temperature and 10 m wind interpolated from the 2 km and 1 km simulations at the same locations are shown as well. During the afternoon of 30 January, the temperature observed along the northeast coast remains below the monthly average temperature by 3 to 4 °C. However, the temperature in the 2 km run is about 1.5 °C higher than the observation. The observation confirms the presence of the cold pool simulated in the 1 km run simulation. Regarding the local circulation, the 10 m wind in the 1 km run exhibits a land breeze behavior after 12:00 UTC, which close to the observations (Fig. 12b), even if the direction of the wind in the morning is difficult to capture by the models.

Cooling associated to precipitation systems is widely reported in the literature. For example, the cold pool observed within or behind well-organized convection is usually explained by sublimation, melting, evaporation cooling and drags of precipitation (Corfidi, 2003). Numerical simulations focusing on the island of Hawaii (Yang and Chen, 2008) indicated that the cooling by orographic clouds during the day and the long-wave radiation heat loss at night have critical impacts on precipitation. To further investigate the cold pool origin during our simulation, we disabled the evaporation process in the numerical model and repeated the simulations at 1 km resolution for the last day. This simulation will be referred to as 1 km (NO EVA) hereafter. The wind field and potential temperature at 950 hPa in the 1 km (NO EVA) are illustrated in

Fig. 13a. It is remarkable that the simulation at 1 km resolution without evaporation process misses the cold pool phenomenon. The precipitation pattern in this run is shifted to the volcanic area and little rainfall is produced over the north-east coastal area (Fig. 13b and c). These results suggest that the microphysical process at 1 km scale is important to well simulate the cooling process caused by evaporation. The atmospheric stability is calculated from the radiosonde in Mauritius (150 km to the east of La Réunion). Taking 1500 m as the average topography height of the island, we obtain the Froude number equal to 0.97 on the last day. The partial blocking condition further promotes the accumulation of the cold air over the coastal area (Houze et al., 2001). The deep convection triggered by the cold pool through thermal lifting and convergence enforces the cloud formation near the coast. The short wave radiation during daytime is further reduced by the cloud. Figure 14 shows the simulated short-wave radiation arriving on surface at 12:00 UTC on 30 January for the 2 km, 1 km and 1 km without evaporation runs. We find a weak solar radiation zone corresponding well to the cold pool in the 1 km run, and a high solar radiation coastal zone in the 2 km and no evaporation cases. This positive cooling feedback is probably important to simulate correctly the precipitation over the coastal area as well.

5 Conclusions

A heavy precipitating event occurring over La Réunion during the summer of 2011 (27–30 January) has been simulated by the French non-hydrostatic mesoscale atmospheric model Meso-NH at four different horizontal resolutions: 4 km, 2 km, 1 km and 500 m. An assessment based on the intense raingauges network shows significant improvement on the 48 and 24 h cumulative rainfall by reducing the model grid spacing from 4 km to 1 km. Both the spatial distributions of these rain fields and the extreme rainfall amounts at particular locations are better represented in the 1 km and 500 m runs. The improvement by reducing model resolution is more apparent for the intense rainfall occurring over the windward coastal area, where the coarser resolution runs (4 km and 2 km) significantly underestimate the precipitation and produce a large spatial error for such extreme precipitation. Regarding the 12 h and 6 h rainfall, all configurations fail to reproduce correctly such temporal variability. A larger parent domain which can well cap-

ture the synoptic circulation evolution at fine temporal resolution will be expected to increase the simulation performance. We found also little improvement between the 1 km and 500 m simulations based on current raingauge network. Rainfall observation at higher resolution is necessary to evaluate these simulations. The radar quantitative precipitation estimation using advanced statistical method, such as the near-neighbors approach (Roberts and Lean, 2008), or a wavelet decomposition approach (Casati et al., 2004; Bousquet et al., 2006), will be needed for the assessment in the future.

The physical mechanism represented by the higher, but not with the lower resolutions has been investigated. A cold pool generated by evaporation appears over the coastal area. The temperature contrast between the ocean and the cold pool creates an offshore circulation and a convergence to the north-east of the island. The moist air coming from the ocean is lifted by the cold pool and produces heavy precipitation in the coastal area. This cold pool may be further enforced by the convective clouds which reduce the solar radiation at the surface. Both the stability of the atmosphere and the mountain blocking process play a potential role to accumulate the cold air along the coast. However, with the coarse resolution simulations (4 km and 2 km), the moist air from ocean reach the interior of island and convection is only triggered by orographic lifting. As a result, their simulation of extreme rain position failed.

Our study showed that the air mixing at 1 km scale in a convective system is important to represent the evaporation process and the cold pool in La Réunion Island. The high-resolution model behaviors under other weather regimes (such as tropical cyclone) at La Réunion Island will be studied in the future.

Acknowledgements. This work was supported by the Fondation MAIF under the PRECYP grant. The simulation was performed using HPC resources from GENCI-CINES (Grant 2013-c2013016660) and from Météo-France. All authors thank the climatology team of Météo-France at La Réunion for providing the observation data and for their constructive suggestions during the task.

References

Bélair, S. and Mailhot, J.: Impact of horizontal resolution on the numerical simulation of a midlatitude squall line: implicit versus explicit condensation, Mon. Weather Rev., 129, 2362–2376, 2001.

Bell, V. A. and Moore, R. J.: The sensitivity of catchment runoff models to rainfall data at different spatial scales, Hydrol. Earth Syst. Sci., 4, 653–667, doi:10.5194/hess-4-653-2000, 2000.

Bernardet, L. R., Grasso, L. D., Nachamkin, J. E., Finley, C. A., and Cotton, W. R.: Simulating convective events using a high-resolution mesoscale model, J. Geophys. Res., 105, 14963–14982, 2000.

Bryan, G. H., Wyngaard, J. C., and Fritsch, J. M.: Resolution requirements for the simulation of deep moist convection, Mon. Weather Rev., 131, 2394–2416, 2003.

Bousquet, O., Lin, C. A., and Zawadzki, I.: Analysis of scale dependence of quantitative precipitation forecast verification: a case-study over the Mackenzie river basin, Q. J. Roy. Meteor. Soc., 132, 2107–2125, 2006.

Casati, B., Ross, G., and Stephenson, D. B.: A new intensity-scale approach for the verification of spatial precipitation forecasts, Meteorol. Appl., 11, 141–154, 2004.

Chan, S. C., Kendon, A., Fowler, H. J., Blenkinsop S., Ferro, C. A. T., and Stephenson D. B.: Does increasing the spatial resolution of a regional climate model improve the simulated daily precipitation?, Clim. Dynam., 41, 1475–1495, 2013.

Colle, B. A., Wolfe, J. B., Steenburgh, J. W., Kingsmill, D. E., Cox, J. A. W., and Shafer, J. C.: High-resolution simulations and microphysical validation of an orographic precipitation event over the Wasatch Mountains during IPEX IOP3, Mon. Weather Rev., 13, 2947–2971, 2005.

Corfidi, S. F.: Cold Pools and MCS propagation: forecasting the motion of downwind-developing MCSs, Weather Forecast., 18, 997–1017, 2003.

Craig, G. C. and Dornbrack, A.: Entrainment in cumulus clouds: what resolution is cloud-resolving, J. Atmos. Sci., 65, 3978–3988, 2008.

Cuxart, J., Bougeault, P., and Redelsperger, J. L.: A turbulence scheme allowing for mesoscale and large-eddy simulations, Q. J. Roy. Meteor. Soc., 126, 1–30, 2000.

Delrieu, G., Andrieu, H., and Creutin, J. D.: Quantification of path-integrated attenuation for X- and C-band weather radar systems operating in heavy rainfall, J. Appl. Meteorol., 39, 840–850, 2000.

Done, J., Davis, C. A., and Weisman, M.: The next generation of NWP: explicit forecasts of convection using the weather research and forecasting (WRF) mode., Atmos. Sci. Lett., 5, 110–117, 2004.

Honnert, R., Masson, V., and Couvreux, F.: A diagnostic for evaluating the representation of turbulence in atmospheric models at the kilometric scale., J. Atmos. Sci., 68, 3112–3131, 2011.

Houze, R. A., James., C. N., and Medina, S.: Radar observations of precipitation and airflow on the Mediterranean side of the Alps: autumn 1998 and 1999, Q. J. Roy. Meteor. Soc., 127, 2537–2558, 2001.

Kain, J. S., Weiss, S. J., Bright, D. R., Baldwin, M. E., Levit, J. J., Carbin, G. W., Schwartz, C. S., Weisman, M. L., Droegemeier, K. K., Weber, D. B., and Thomas, K. W.: Some practical considerations regarding horizontal resolution in the first generation of operational convection-allowing NWP, Wea. Forecasting, 23, 931–952, 2008.

Kendon, E. J., Roberts, N. M., Senior, C. A., and Roberts, M. J.: Realism of rainfall in a very high-resolution regional climate model, J. Climate, 25, 5791–5806, 2012.

Kobold, M. and Sušelj, K.: Precipitation forecasts and their uncertainty as input into hydrological models, Hydrol. Earth Syst. Sci., 9, 322–332, doi:10.5194/hess-9-322-2005, 2005.

Lafore, J. P., Stein, J., Asencio, N., Bougeault, P., Ducrocq, V., Duron, J., Fischer, C., Héreil, P., Mascart, P., Masson, V., Pinty, J. P., Redelsperger, J. L., Richard, E., and Vilà-Guerau de Arellano, J.: The Meso-NH Atmospheric Simulation System. Part I: adiabatic formulation and control simulations, Ann. Geophys., 16, 90–109, doi:10.1007/s00585-997-0090-6, 1998.

Luna, T., Rocha, A., Carvalho, A. C., Ferreira, J. A., and Sousa, J.: Modelling the extreme precipitation event over Madeira Island on 20 February 2010, Nat. Hazards Earth Syst. Sci., 11, 2437–2452, doi:10.5194/nhess-11-2437-2011, 2011.

Mass, C. F., Ovens, D., Westrick, K., and Colle, B. A.: Does increasing horizontal resolution produce more skillful forecasts?, B. Am. Meteorol. Soc., 83, 407–430, 2002.

Montroty, R., Rabier, F., Westrelin, S., Faure, G., and Viltard, N.: Impact of wind bogus and cloud and rain affected SSM/I data on tropical cyclones analyses and forecasts, Q. J. Roy. Meteor. Soc., 134, 1673–1699, 2008.

Pellarin, T., Delrieu, G., Saulnier, G. M., Andrieu, H., Vignal, B., and Creutin, J. D.: Hydrologic visibility of weather radar systems operating in mountainous regions: case study for the Ardèche catchment (France), J. Hydrometeorol., 3, 539–555, 2002.

Pergaud, J., Masson, V., Malardel, S., and Couvreux, F.: A parameterization of dry thermals and shallow cumuli for mesoscale numerical weather prediction, Bound.-Lay. Meteorol., 132, 83–106, 2009.

Petch, J. C.: Sensitivity studies of developing convection in a cloud-resolving model, Q. J. Roy. Meteor. Soc., 132, 345–358, 2006.

Petch, J. C., Brown, A. R., and Gray, M. E. B.: The impact of horizontal resolution on the simulations of convective development over land, Q. J. Roy. Meteor. Soc., 128, 2031–2044, 2002.

Pinty, J. P. and Jabouille, P.: A mixed-phase cloud parameterization for use in mesoscale non-hydrostatic model: simulations of a squall line and of orographic precipitation, in: Proc. Conf. of Cloud Physics, Everett, WA, USA, Am. Meteorol. Soc., 217–220, 1998.

Quetelard, H., Bessemoulin, P., Cerveny, R. S., Peterson, T. C., Burton, A., and Boodhoo, Y.: Extreme weather: world-record rainfalls during topical cyclone Camede, B. Am. Meteorol. Soc., 90, 603–608, 2009.

Ricard, D., Lac, C., Riette, S., Legrand, R., and Mary, A.: Kinetic energy spectra characteristics of two convection-permitting limited-area models AROME and Meso-NH, Q. J. R. Meteorol. Soc., 139, 1327–1341, 2013.

Réchou, A., Plu, M., Campistron, B., and Decoupes, R.: One-year analysis of rain and rain erosivity in a tropical volcanic island from UHF wind profiler measurements, Atmos. Meas. Tech. Discuss., 6, 3249–3277, doi:10.5194/amtd-6-3249-2013, 2013.

Roberts, N. M. and Lean, H. W.: Scale-selective verification of rainfall accumulations from high-resolution forecasts of convective events, Mon. Weather Rev., 136, 78–97, 2008.

Seity, Y., Brousseau, P., Malardel, S., Hello, G., Bénard, P., Bouttier, F., Lac, C., and Masson, V.: The AROME-France convective-scale operational model, Mon. Weather Rev., 139, 976–991, 2011.

Schwartz, C. S., Kain, J. S., Weiss, S. J., Xue, M., Bright, D. R., Kong F., Thomas, K. W., Levit, J. J., and Coniglio, M. C.: Next-Day convection-allowing WRF model guidance: A second look at 2-km versus 4-km grid spacing. Mon. Wea. Rev., 137, 3351–3372, 2009.

Smith, S. A., Vosper, S. B., and Field, P. R.: Sensitivity of orographic precipitation enhancement to horizontal resolution in the operational Met Office Weather forecasts, Meteorol. Appl., in press, doi:10.1002/met.1352, 2012.

Stein, J., Richard, E., Lafore, J. E., Pinty, J. P., Asencio, N., and Cosma, S.: High-resolution non-hydrostatic simulations of flash-flood episodes with grid-nesting and ice-phase parameterization. Meteor. Atmos. Phys., 72, 203–221,2000.

Tetzlaff, D. and Uhlenbrook, S.: Significance of spatial variability in precipitation for process-oriented modelling: results from two nested catchments using radar and ground station data, Hydrol. Earth Syst. Sci., 9, 29–41, doi:10.5194/hess-9-29-2005, 2005.

Weisman, M. L., Skamarock, W. C., and Klemp, J. B.: The resolution dependence of explicitly modeled convective systems, Mon. Weather Rev., 125, 527–548, 1997.

Yang, C. and Chen, Y. L.: Effect of terrain heights and sizes on island-scale circulations and rainfall for the island of Hawaii during HaRP, Mon. Weather Rev., 136, 120–146, 2008.

Younis, J., Anquetin, S., and Thielen, J.: The benefit of high-resolution operational weather forecasts for flash flood warning, Hydrol. Earth Syst. Sci., 12, 1039–1051, doi:10.5194/hess-12-1039-2008, 2008.

Yu, N., Boudevillain, B., Delrieu, G., and Uijlenhoet, R.: Estimation of rain kinetic energy from radar reflectivity and/or rain rate based on a scaling formulation of the raindrop size distribution, Water Resour. Res., 48, W04505, doi:10.1029/2011WR011437, 2012.

Zhang, M. and Zhang, D. L.: Subkilometer simulation of a torrential-rain-producing mesoscale convective system in East China. Part I: Model verification and convective organization, Mon. Weather Rev., 140, 184–201, 2012.

Table 1. Configuration and grids definition in different numerical runs.

Abbr.		4 km	2 km	1 km	500 m
Grid (pts × pts)	D1	90×90	180×180	180×180	180×180
	D2	–	–	80×72	160×144
Resolution (km)	D1	4	2	2	2
	D2	–	–	1	0.5
Time step (s)	D1	8	4	4	4
	D2	–	–	2	1
Turbulence scheme	D1	1D	1D	1D	1D
	D2	–	–	3D	3D
Nesting		–	–	2-way	2-way

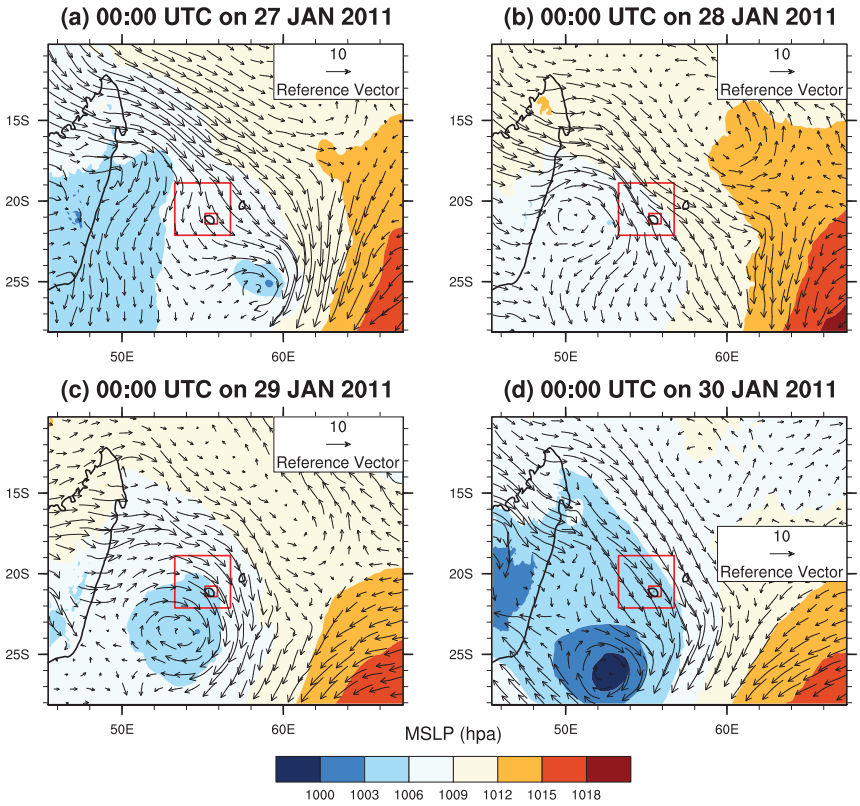

Fig. 1. Mean sea level pressure (hPa) and horizontal wind ($\mathrm{m/s}$) at 850 hPa obtained from the Aladin-Réunion analyses at 00:00 UTC on 27 **(a)**, 28 **(b)**, 29 **(c)** and 30 **(d)** January. The red rectangles represent the two Meso-NH domains simulations: D1 (large one), D2 (small one).

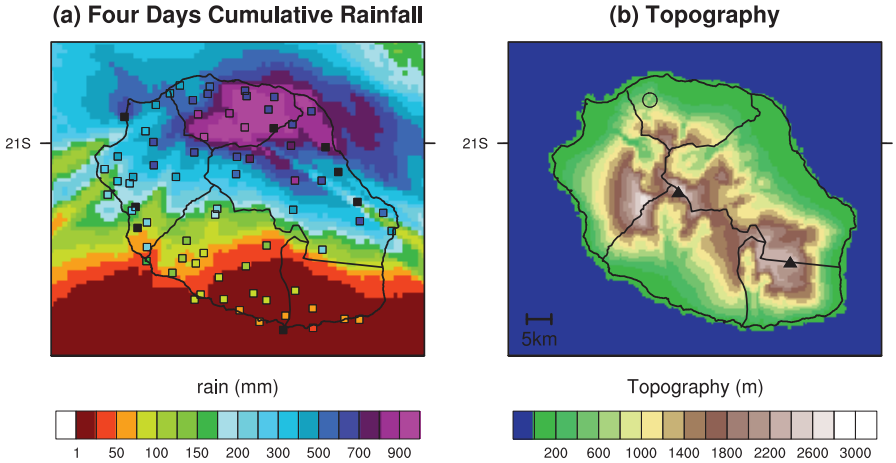

Fig. 2. (a) Cumulative precipitation (in mm) during the four days measured by raingauges (squares) and estimated by the weather radar (colored areas). A black square means that there is at least one-hour missing record at such rain station. **(b)** Topography of La Reunion (in m) with five areas (N, W, S, SE and NE) defined by the local disaster management service. The location of the weather radar is indicated by the circle and the black triangles represent the Piton de la Fournaise at the south-east and Piton des Neiges in the center.

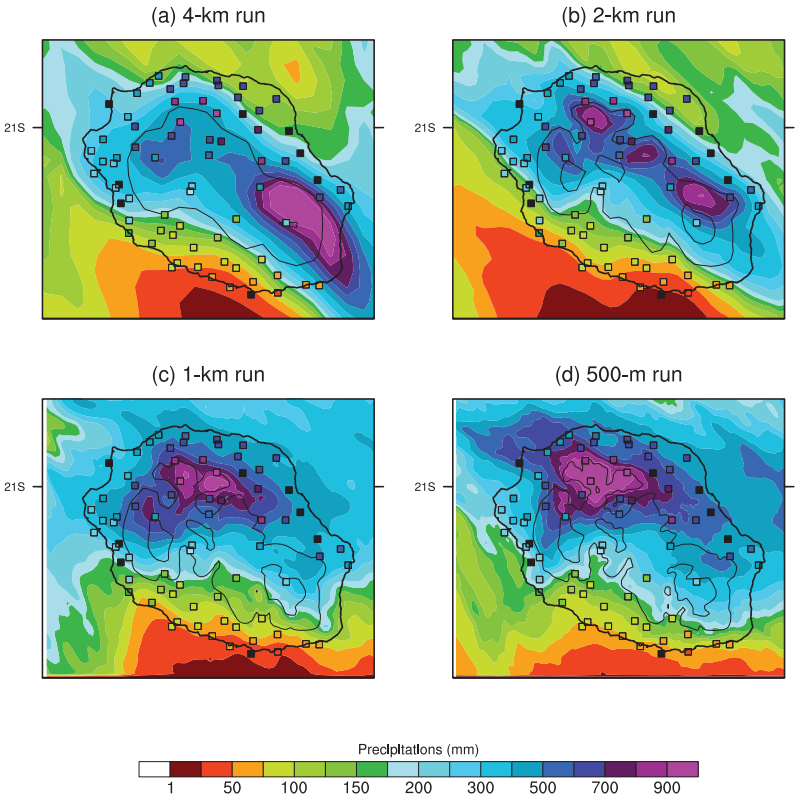

Fig. 3. 4 day cumulative rainfall (in mm) produced by the **(a)** 4 km, **(b)** 2 km, **(c)** 1 km and **(d)** 500 m simulations (colored area), superimposed with the raingauges measurements (squares). The black contours display the 1000 m and 2000 m altitude isolines as reproduced by the model at different resolutions.

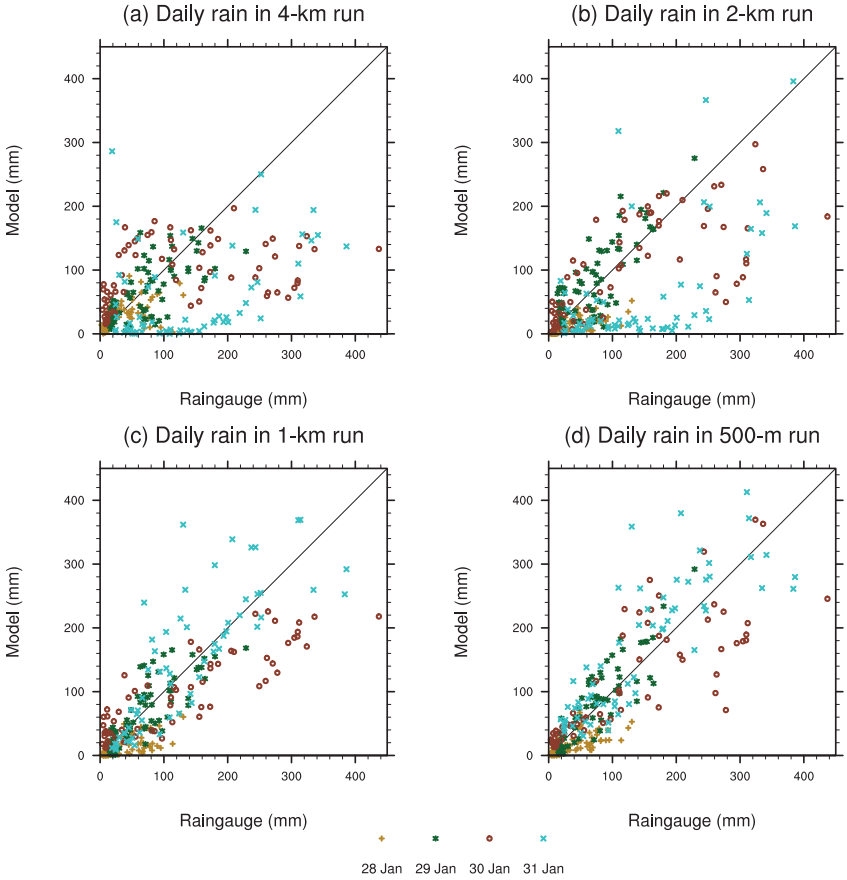

Fig. 4. Simulated vs. observed daily precipitation (in mm) at raingauge locations obtained from the **(a)** 4 km, **(b)** 2 km, **(c)** 1 km and **(d)** 500 m simulations.

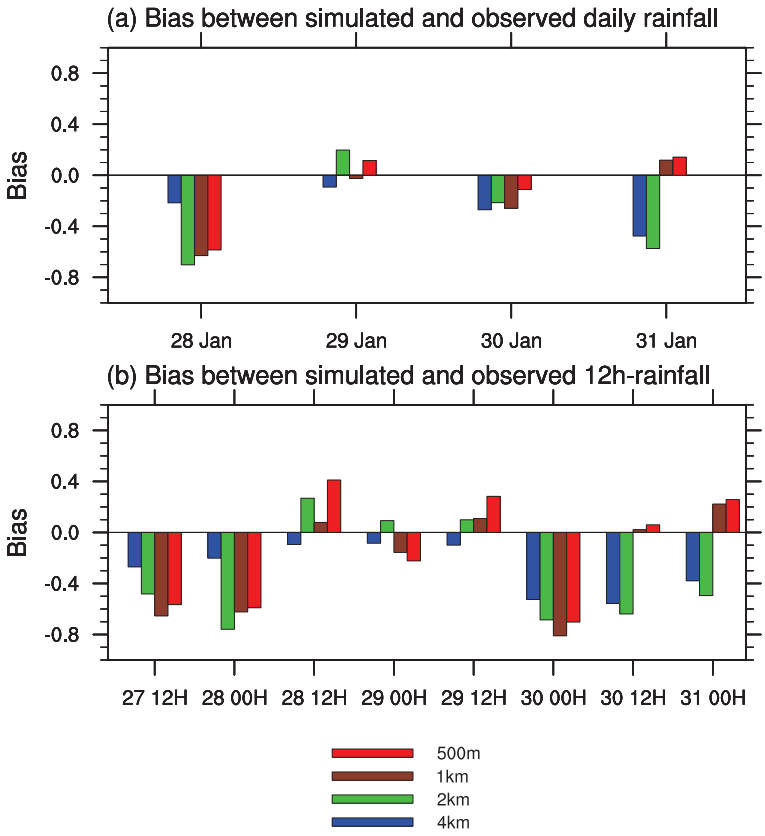

Fig. 5. Bias of simulated rainfall cumulated over **(a)** 24 h and **(b)** 12 h during the four days for the four runs: 4 km (blue bars), 2 km (green bars), 1 km (brown bars) and 500 m (red bars).

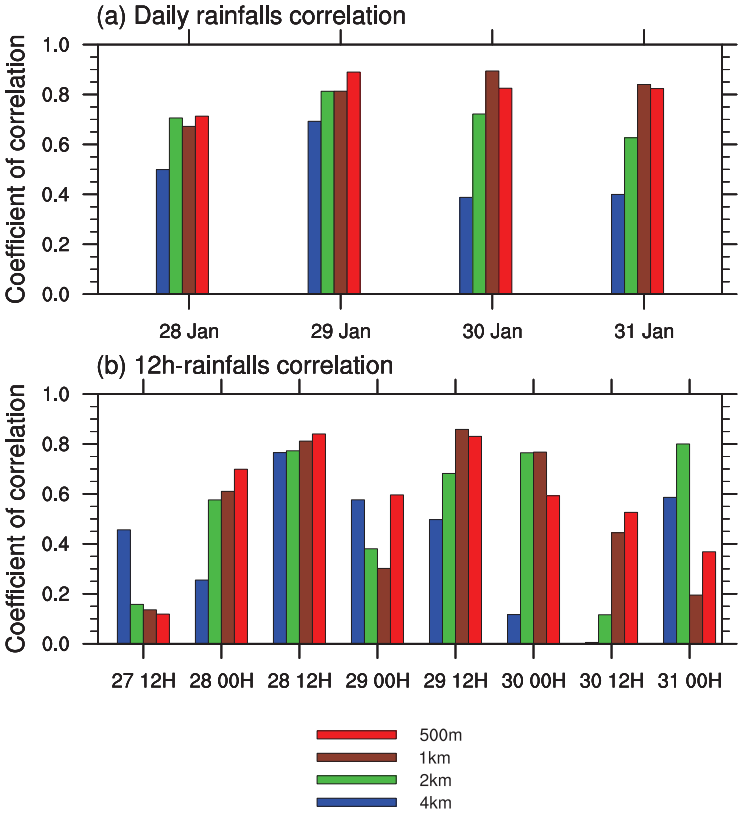

Fig. 6. Spatial correlation coefficient between simulated and observed rainfall (in mm) cumulated over **(a)** 24 h and **(b)** 12 h for the four runs: 4 km (blue bars), 2 km (green bars), 1 km (brown bars) and 500 m (red bars).

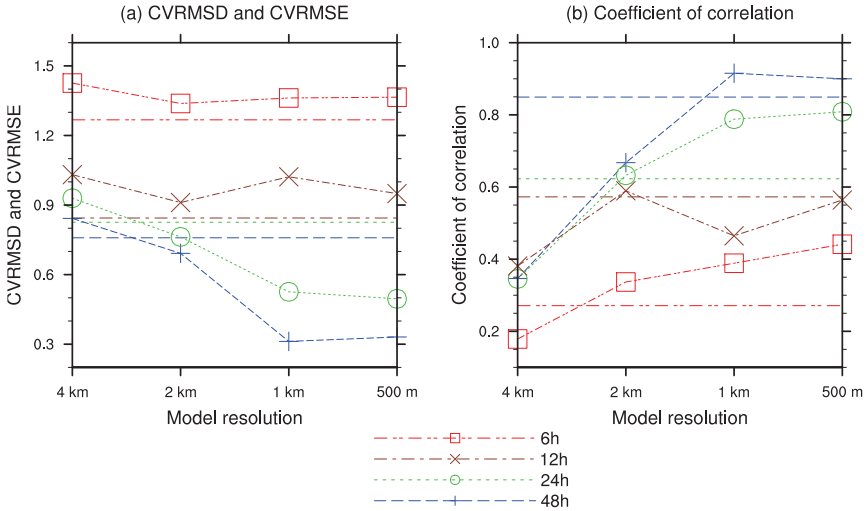

Fig. 7. (a) Coefficient of variation of the root-mean-square error (CVRMSE) and **(b)** coefficient of correlation for different cumulative rainfall periods as a function of model resolution. The dashed lines represent the statistical criteria representing the temporal and spatial variability of rainfall (see Sect. 3.1 for more details).

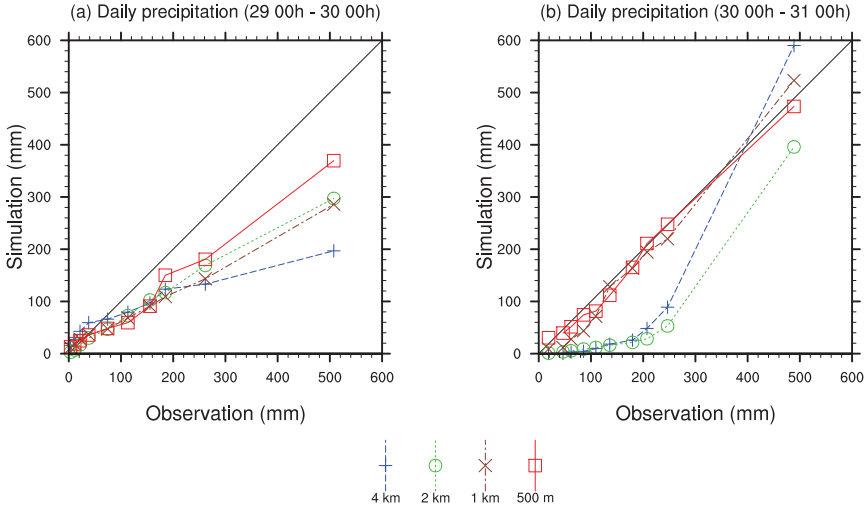

Fig. 8. Quantiles–quantiles diagram for the simulated and observed daily precipitation on the last two days of the event for the 4 km (blue line), 2 km (red line), 1 km (black line) and 500 m (red line) runs.

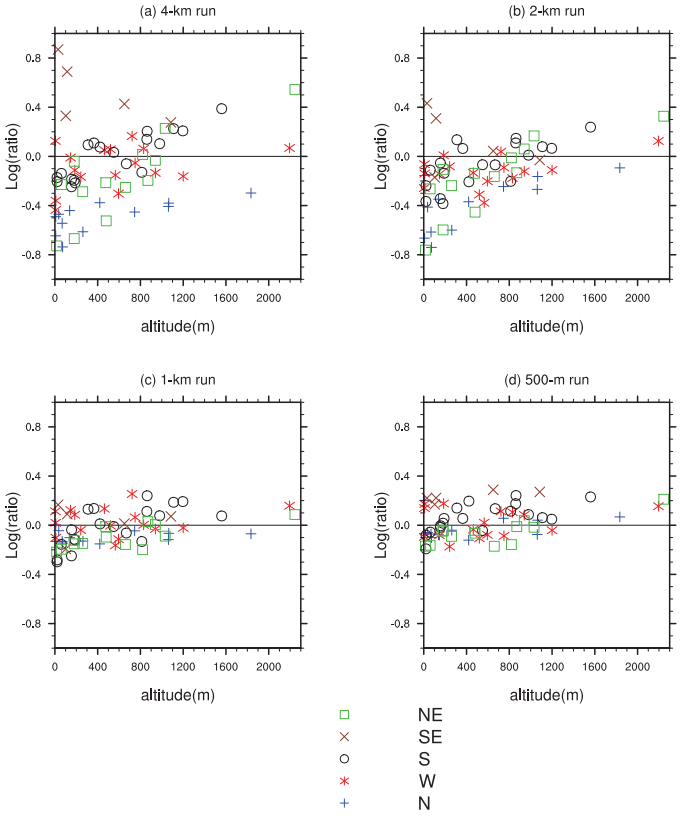

Fig. 9. Bias of 4 day rainfall at each rain gauge station, as a function of the altitude (m) and locations for the **(a)** 4, **(b)** 2, **(c)** 1 and **(d)** 0.5 km runs. The data are divided into 5 geographical zones: NE (green squares), SE (brown crosses), S (black circles), W (red stars) and N (blue +).

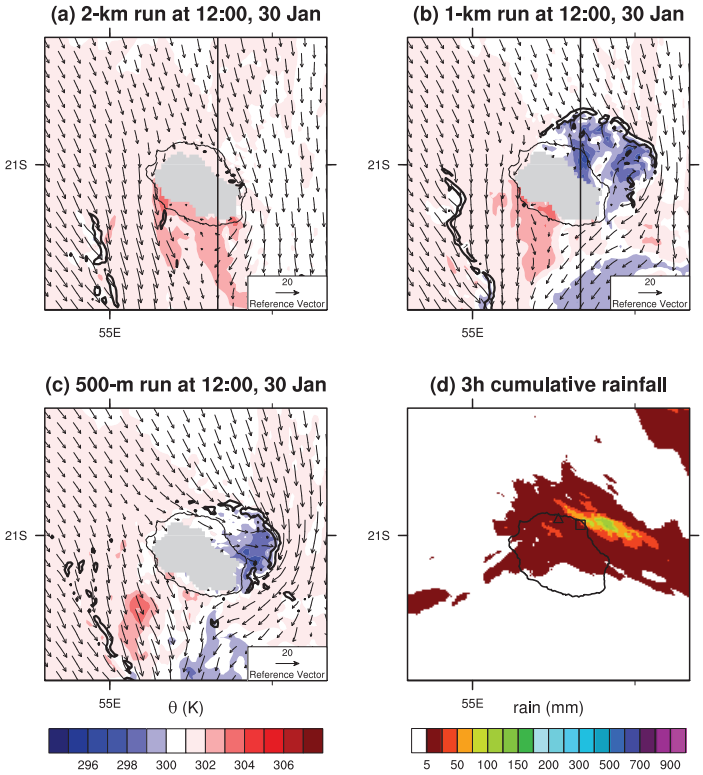

Fig. 10. Simulated horizontal wind field ($\mathrm{m\,s^{-1}}$) and potential temperature (K, colors) at 950 hPa in the **(a)** 2 km, **(b)** 1 km and **(c)** 500 m runs. The black contours represent the vertical velocity at $1\,\mathrm{m\,s^{-1}}$ at 950 hPa. The north-south line segments correspond to the locations of the vertical cross sections in Fig. 11; **(d)** 3 h cumulative rainfall (12:00 to 15:00 UTC; in mm) estimated by radar with the positions of two meteorological stations: Gillot-Airport (triangle) and Le Colosse (square).

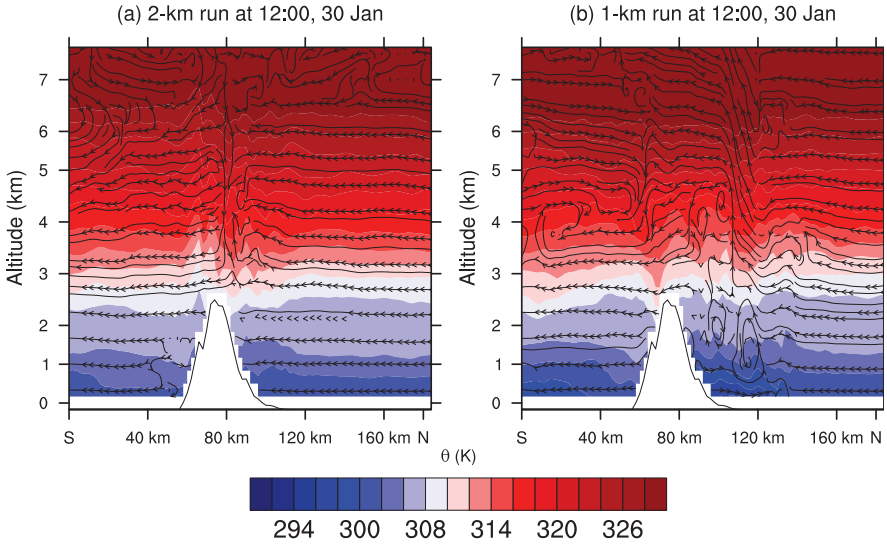

Fig. 11. North-south cross section of wind (vectors) and potential temperature (in K; colors) along the segment defined in Fig. 10, in the **(a)** 2 km and **(b)** 1 km runs on 30 January at 12:00 UTC.

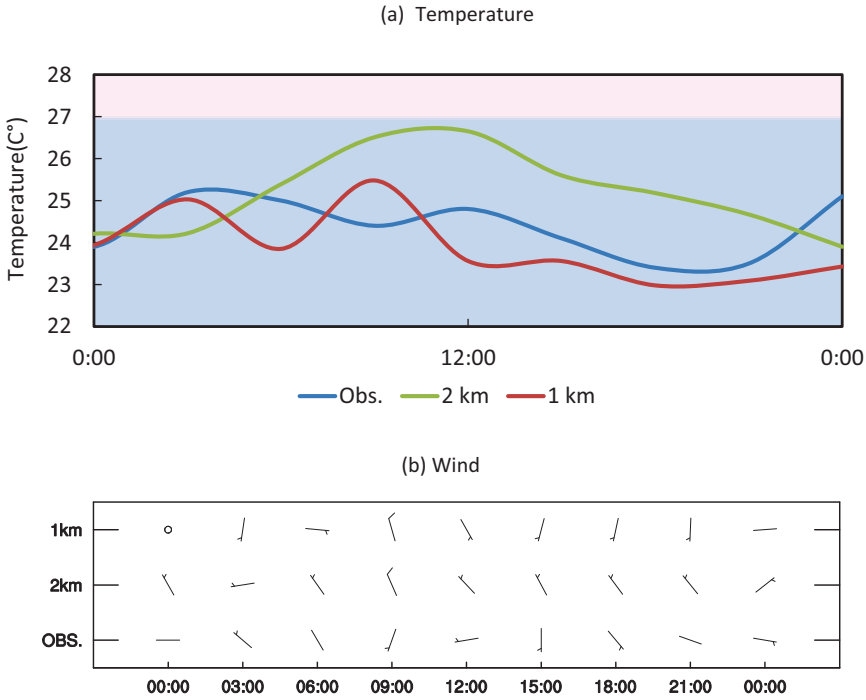

Fig. 12. (a) Average temperature (°C) simulated by the 2 km (green curve) and 1 km (red curve) runs and observed (blue curve) at Le Colosse and Gillot-Airport stations. The background boundary indicates the climatological temperature in January at La Réunion; **(b)** observed and simulated horizontal wind at Gillot-Airport station during the last day of the event.

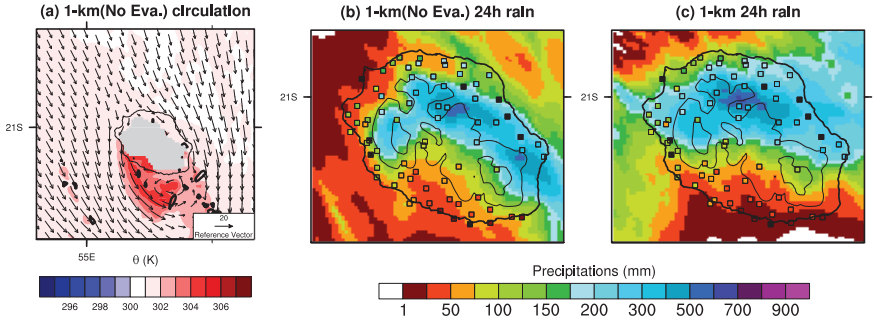

Fig. 13. (a) Same as Fig. 10b, but the evaporation is disabled in the simulation. Daily precipitation on the last day of the event simulated by the 1 km (No EVA) run in **(b)**, and by the reference 1 km run in **(c)**. Raingauges measurements are represented by colored squares.

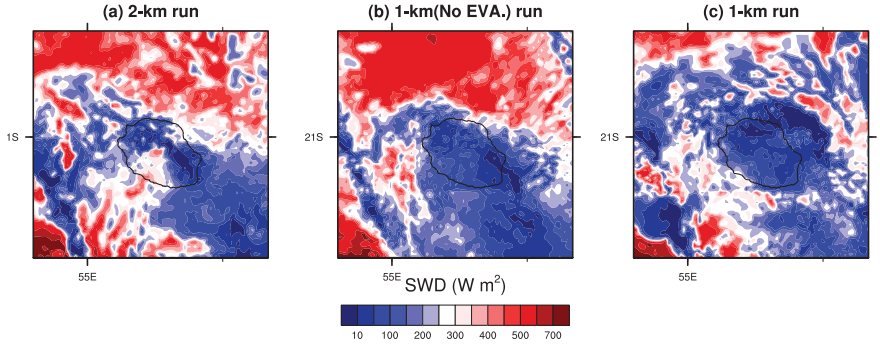

Fig. 14. Shortwave radiation ($\mathrm{W\,m^{-2}}$) simulated by the **(a)** 2 km, **(b)** 1 km (No EVA) and **(c)** 1 km runs at 12:00 UTC on 30 January 2011.